

Spectral characteristics of high latitude raw 40MHz cosmic noise signals

C. M. Hall¹

¹Tromsø Geophysical Observatory, The Arctic University of Norway, Norway

5

Corresponding author:

C. M. Hall, chris.hall@uit.no

Full institute address:

10 UiT - The Arctic University of Norway
Tromsø Geophysical Observatory
9037 Tromsø
Norway

15

Abstract

Cosmic noise at 40MHz is measured at Ny-Ålesund (79°N, 12°E) using a relative ionospheric opacity meter (“riometer”). A riometer is normally used to determine the degree to which cosmic noise is absorbed by the intervening ionosphere, giving an indication of ionization of the atmosphere at altitudes lower than generally monitored by other instruments. The usual course is to determine a “quiet-day” variation, this representing the galactic noise signal itself in the absence of absorption; the current signal is then subtracted from this to arrive at absorption expressed in dB. By a variety of means and assumptions, it is thereafter possible to estimate electron density profiles in the very lowest reaches of the ionosphere. Here however, the entire signal, i.e. including the cosmic noise itself will be examined and spectral characteristics identified. It will be seen that distinct spectral subranges are evident which can, in turn be identified with non-Gaussian processes characterized by generalized Hurst exponents, α . Considering all periods greater than 1 hour, $\alpha \approx 1.24$ – an indication of fractional Brownian motion, whereas for periods greater than 1 day $\alpha \approx 0.9$ - approximately pink noise and just in the domain of fractional Gaussian noise. The results are compared with other physical processes suggesting that *absorption* of cosmic noise is characterized by a generalized Hurst exponent ≈ 1.24 and thus non-persistent fractional Brownian motion, whereas *generation* of cosmic noise is characterized by a generalized Hurst exponent ≈ 1 .

1. Introduction and instrumentation

The relative ionospheric opacity meter (“riometer”) is a traditional instrument for measuring the degree to which cosmic noise is absorbed by the ionosphere (e.g. Little and Leinbach, 1959). By selecting a particular frequency for the riometer reception, it is possible to optimize the sensitivity to a particular altitude range and therefore how energetic the particles are that are causing the ionization. The means of analyzing the signal from the riometer is to determine the “quiet day” variation and thereafter the degree of absorption caused by the intervening ionosphere. For a given radio wave frequency, the transmission, total reflection, partial reflection or absorption is indicated by the refractive index of the atmosphere. The refractive index of an ionized medium is in turn related to plasma parameters and the frequency of the radio wave in question by the Appleton-Hartree equation; this is thus a starting point for understanding the response of the riometer signal to varying degrees of particle precipitation (Hargreaves, 1979 and 1992). Here, however the signal in its original form, as opposed to the derived absorption, will be examined, i.e. the cosmic noise as measured by a receiver at the Earth’s surface, since the object of this study is to investigate the spectrum of the signal itself including intermittency introduced by solar activity.

Data have been obtained from the recently established 40MHz single beam riometer at Ny-Ålesund (79°N, 12°E), this being particularly undisturbed due to stringent restrictions on local activity such as use of radio and traffic. On the other hand, the location is well within the polar cap and the ionosphere is less disturbed by auroral activity than at, say, 70°N. The use of 40MHz furthermore makes the instrument less sensitive to less energetic particles than, for example a 30MHz instrument. Instruments such as the one used here are highly reliable and run unattended with minimal interruption. The riometer at Ny-Ålesund, manufactured by La Jolla Sciences of California, delivers signal strengths measured in mV every 2 seconds.

60 Reception is via a 3-element crossed Yagi antenna having a half-power full-beamwidth of approximately 70° . Localized (with respect to the sky) sources of cosmic noise in the field of view as the Earth rotates are thus smoothed out by the wide antenna beam, and the undisturbed cosmic noise signal is therefore manifested by a smooth quasi-sinusoidal variation with period of one sidereal day (0.99726958 mean solar days). In general, the signal
65 is characterized by this dominant variation. The amplitude of the sidereal diurnal variation varies with latitude, being zero at the pole (where the sky view is independent of time-of-day) and maximum at the equator. In addition, the quasi-sinusoidal signature is modulated by insolation that gives increased ionization during day and furthermore affects negative ion chemistry, a reduction in received cosmic noise occurring when the ionospheric D-region is
70 sunlit. Although a seasonal effect at all latitudes, the degree of insolation changes more significantly at higher latitudes: in mid-winter, the lower D-region is not sunlit at all and vice versa in summer. These predictable periodic (deterministic) variations are discussed in the early reports by Forbush (1954 and 1958), which also contain pointers to similar work of the time, and an example of a more recent report is Behera et al. (2014).

75 As mentioned above, the idea of the riometer is to determine the absorption of cosmic noise due to perturbations in the intervening ionosphere due to space weather effects. These perturbations, in contrast to the largely deterministic quasi-diurnal and longer periods, end to be intra-diurnal and often of only ~hours duration, as for example, an auroral arc passes overhead (again, Hargreaves, 1979 and 1992, and references at the ends of the appropriate
80 chapters). These variations are highly intermittent and can be expected to be as stochastic in nature as, for example, the solar activity that represents the underlying forcing. Finally, observations are typically influenced by local sources of disturbance such as nearby radio emissions and other radio frequency (RF) emissions from, for example, traffic. For the

riometer used in this study, hourly calibration marks are also produced, but these are indeed
85 hourly and therefore predictable. In addition, instrument noise is present to some degree, and
the analogue to digital conversion is only 8-bit resulting in a degree of quantization of the 2-
second resolution readings. Although the riometer reacts instantaneously to ionospheric
enhancement, a typical absorption event evolves over several measurements and therefore 1-
minute smoothing can be applied because in practice an observer would wait perhaps one
90 minute to identify the event unambiguously. The entire dataset is portrayed in Fig. 1. after
applying a 1-month running mean in order to illustrate the seasonal variation. Data from
December 2013 to May 2015 are used in this study, again using the 40MHz riometer at 70°N,
19°E. To illustrate the features described above, one day of data (20 September 2014) are
plotted in Fig. 2., in which the 8-bit quantization can be seen together with the hourly
95 calibration (normally negative) spikes. The sidereal-day variation is the obvious overall
feature, and when successive calendar days are plotted, the phase is seen to migrate to the left
by approximately 4 minutes per day. The absorption events at 1330 and 1500 are well
identified. The first absorption event is short-lived (~1 hour) whereas the second event is
longer, evidently continuing through the rest of the day. It should be stressed that these
100 individual events per se are not the subject of this study, Figs. 1 and 2 merely illustrate the
long-and short-term variations in the dataset. In the following sections, the spectral
characteristics of the entire dataset will be examined and discussed, thus including the
deterministic periodicities and the collection of intermittent absorption events. The
intermittent and short timescale nature of the ionospheric disturbances are expected to be
105 manifested by spectral characteristics different from the more predictable cosmic noise
background. The former can ultimately be traced back to solar variability (popularly referred
to as “space weather”) and the latter traced to galactic variability, or rather the riometer’s

varying view of the galactic sources. As a major feature of the discussion, the non-Gaussian nature of the distribution of the stochastic part of the signal will be addressed.

110 A significant problem in the study of physical systems is the identification of coupling between processes, what are causes and what are true effects. An evolving approach is to examine the stochastic nature of the signals from different processes because noise present in a cause will presumably be also present in resulting effects. The noise signatures may not be unambiguous of course, so any apparent coupling must be treated with care. Although

115 gaining popularity, the principle was introduced by, inter alios, Hurst, (1951), Mandelbrot, (1983), Grassberger and Procaccia, (1983) and Koscielny-Bunde et al. (1998) and later explored by (e.g.) Eichner et al. (2003), Lennartz and Bunde (2009), Kantelhardt et al. (2006), Rypdal and Rypdal (2011), Hall (2014a and b). The concepts of fractional Gaussian noise (fGn) and fractional Brownian motion (fBm) have been proposed by Mandelbrot and

120 van Ness (1968), and the Hurst exponent, H , by Hurst, (1951) all to help quantify self-affinity of stochastic components of time-series. For fBm, successive increments are correlated resulting from the time-series being non-stationary and with temporally changing variance; for fGn, the time-series is stationary and expectation value and variance are time-invariant. The Hurst exponent is not able to differentiate between these processes, however, and here

125 the approach of Kantelhardt et al. (2006) is adopted to derive rather the *generalized Hurst exponent*, α . The two exponents are related: for fGn, $H = \alpha$ and for fBm, $H = \alpha - 1$. The exponent α unambiguously characterizes the process as fBm ($\alpha > 1$), or fGn ($0 < \alpha < 1$). Furthermore, a process can be described as anti-persistent when an increment is likely to be followed by one in the reverse direction: for fGn, $0 < \alpha < 0.5$ and for fBm $1 < \alpha < 1.5$. On the

130 other hand, a process is persistent when an increment is more likely to be followed by one in the same direction: for fGn, $0.5 < \alpha < 1.9$ and for fBm $\alpha > 1.5$. The case $\alpha = 1.5$ indicates the

(well-known) special case of Brownian motion. One method to determine α is first to find the scaling exponent β of the power spectrum $S(f)$, f being frequency:

$$S(f) \propto |f|^{-\beta} \quad (1)$$

Thereafter, the *generalized Hurst exponent*, α is related to β by

$$\alpha = (\beta + 1)/2 \quad (2)$$

135 the derivation of which can be found in, e.g., Hartmann et al. (2013), and Delignieres et al. (2006), and references therein.

Using the approach of Hall (2014a,b), the stochastic component of the time-series is isolated from the slowly evolving (deterministic) component. Here, a smoothed time-series will be subtracted from the original and the residual will be deemed stochastic, as will be
 140 demonstrated in the following section. From the stochastic (noise) component, the probability density function (PDF) of the data is obtained and thereafter quantile-quantile (Q-Q) analyses (Wilk and Gnanadesikan, 1968) performed. To produce Q-Q plots, quantiles of the distribution of signal noise are plotted against corresponding quantiles for hypothesized distributions exhibiting the same mean and standard deviation. A visual inspection of the
 145 PDF can indicate if the signal's noise distribution is Gaussian or otherwise. From an inspection of the Q-Q plots the degree to which the signal's noise distribution agrees with that hypothesized: a straight line indicating agreement.

In this study, the goal is to investigate the spectrum of the cosmic noise data in its entirety, encompassing variations at all timescales and see if well-defined subranges exist that can be
 150 related to known physics. The starting point is not, therefore a derived stochastic component. Furthermore, experimental data, including gaps due to instrument failure are almost

invariably irregularly sampled and therefore the Lomb-Scargle periodogram analysis (Press and Rybicki, 1989) will be used rather than a traditional Fourier transform. Fougère (1985) and Eke et al. (2000) propose preconditioning of the time series by applying a parabolic window, thereafter bridge detrending using the first and last points in the series, and then a final frequency selection before identifying subranges exhibiting linear dependence in log-log space. This last step however will be omitted in order to retain as much spectral information as possible, at least initially.

It should be mentioned that several approaches are available for estimating H or α , the most popular perhaps being the detrended fluctuation analysis (DFA) (Peng et al. 1993). Physicists in general are familiar with spectral analyses, this being the focus here. For reference, commonly used methods including spectral analysis (SA) have been described by Delignieres et al. (2006), Hartmann et al. (2013) and Heneghan and McDarby (2000).

2. Analyses

As described in the previous section, an approximation to the stochastic component of the cosmic noise signal is extracted from the complete dataset. Which timescales contain deterministic signals is open to discussion; since perturbations resulting from solar-terrestrial interaction can recur over periods of days (such as some polar cap absorption events), the time series shown in Fig. 1. has been deemed deterministic. This is then subtracted from the original and the residual deemed largely stochastic. A corresponding method was employed by Hall (2014b). As will be seen, spectral analysis identifies individual periodicities remaining in the (supposedly) stochastic residual, these showing up as narrow spikes. Due to the large number of data points and therefore frequencies in the spectrum, these spikes impose insignificant influence when determining the spectral slope. A disadvantage with DFA is that such periodicities are generally *not* easily distinguishable.

A number of studies have hypothesized that solar fluctuations give rise to processes that may be characterized by Lévy walks or flights, e.g. Scafetta and West (2003) and Watkins et al. (2005) (and references therein). As explained by Sato (1999), a Cauchy process is defined as Brownian motion subordinated to a process associated with a Lévy distribution. The earlier
180 analyses of solar and ionospheric observables are therefore considered a justification for comparing a Cauchy distribution as well as Gaussian with that of the riometer data. The probability density function (distribution) of the stochastic component of the data is determined and shown in Fig. 3. The distribution is centred on zero resulting from subtraction of the deterministic component. A Gaussian distribution is fitted that fails to reproduce the
185 narrowness of the distribution of the observation at half height. By using a different parameterization of the distribution width than half-maximum full-width, viz. $1/e$ of maximum, a wider Cauchy distribution is modelled that fits the data better (suggested by Hall, 2014b). Qualitatively the Cauchy model describes the distribution considerably better than the Gaussian, but all the same, a heavy “shoulder” is evident for reduced values of
190 cosmic noise. The centre and right panels of Fig. 3. show the quantile-quantile (Q-Q) portrayals –vs. Gaussian (centre) and vs. Cauchy (right). The means of interpreting such Q-Q plots are described by Chambers et al. (1963). Departures from linearity (in the central regions of the plots) indicate heavy shoulders at both sides (sometimes referred to as long tails) of the distribution relative to the model. It can be seen that the Cauchy model
195 approaches the shoulders in the distribution of the measurement somewhat better than the Gaussian. In fact, a Cauchy model will always represent the long tails in a distribution better than a Gaussian as can be seen in the left-hand panel. The portrayals in Fig. 3. point to a Lévy process being the best description of the stochastic component rather than Gaussian noise.

For determination of power spectral density, the entire original dataset is employed, such that
200 all conceivable fluctuations are included. There are therefore no a priori assumptions as to
which fluctuations are truly non-chaotic. The exception is the sidereal periodicity, but as
stated earlier, this represents but one narrow spike in the spectrum compared with all other
frequencies present and does not influence the identification of subranges exhibiting scaling
and subsequent determination of exponents β . Prior to spectral analysis, the data are
205 preconditioned by applying a parabolic window and then bridge detrending using the first and
last points as described in the previous section. Thereafter, the Lomb-Scargle periodogram
analysis is applied, again as explained earlier. The result is shown in Fig. 4. In reality, a
considerable amount of (approximately) white noise results at periods shorter than 1 minute
and these are associated with instrumental noise and quantization of measurements due to the
210 use of an 8-bit analogue-to-digital converter. The first indication of this instrumental noise is
seen at the very right-hand end of the plot, and the remainder is omitted in order not to detract
from the characteristics of the received signal itself. Meaningful timescales are indicated on
the figure for the convenience of the reader: 1 minute, 1 hour and 1 day, the last being the
sidereal day. The scaling is quite evident, although delineation of separate subranges is
215 somewhat subjective. Since experience shows that, for example, auroral activity in the field
of view of such instruments as the riometer (depending of course on the antenna type) last
from typically minutes to hours, linear fits to the log-log spectrum have been performed for
all periods greater than 1 minute, 1 hour and 1 sidereal day. Slopes and uncertainties were
obtained using least-squares fitting (in log-log space) as described by, e.g. Taylor (1982).
220 Due to the high density of points at high frequencies, the longer than 1 min period spectral
regime is heavily weighted towards the 1 hour to 1 min subrange etc. The respective fits are
superimposed on the plot. For periods > 1 min, $\beta = 0.72 \pm 0.001$; for periods > 1 hour, $\beta =$
 1.48 ± 0.006 ; for periods > 1 day, $\beta = 0.87 \pm 0.035$.

Discussion

225 The first characteristic to note is that for all variability in 40MHz cosmic noise at timescales shorter than 1 month, the probability density function is not well represented by a Gaussian distribution. The attempt to fit a Cauchy distribution defining the width being at $1/e$ as opposed to $1/2$ maximum succeeded in matching the heaviness in the tails of the distribution, but not the narrowness on the peak. By definition, the Cauchy distribution is symmetric, and

230 therefore while the model represents the heavy tail for positive values, the presence of the negative shoulder is conveniently accentuated. It should be remembered, however, that the approach is rather simplistic. Qualitatively the distribution is reminiscent of a Lévy process (which is also represented by a Cauchy distribution) but no attempt will be made to sub-classify this further here, the method being fraught with pitfalls (e.g. see Rypdal and Rypdal,

235 2010). Examining the Q-Q plots, the heavy-tailed distribution is characterized by the downward trend at the left-hand ends and upward trend at the right-hand ends of both Gaussian and Cauchy versions. The overall upward curvature in the Cauchy plot indicates a degree of skewness due to the shoulder. Lack of discontinuities indicate lack of bimodal (or multimodal) distributions. Recalling that the above analyses have been performed on the

240 residual after subtracting the smoothed data from the original observation, the negative values in the distribution are associated with reductions in the original signal. Thus, the shoulder in the distribution and the evidence for skewness in the Q-Q plots are readily explained by intra-day absorption events, their intermittent signature contributing to, if not responsible for, the non-Gaussian probability density function.

245 Turning to the spectral analysis, there is an indication that 3 subranges are present in the spectrum. Timescales associated with auroral activity which, in turn correspond to enhanced electron densities in the ionospheric D-region, are typically minutes to hours. One can

envisage an auroral arc moving across the sky; although this will be in one position for a short time interval, it will be in the riometer antenna beam for much longer. The response of a ground-based magnetometer is similar as described by Hall (2014b), although current systems causing perturbations in the geomagnetic field typically occur at higher altitude than ionisation modulating cosmic noise at 40MHz. It can therefore be hypothesized that the scaling exponent for periods > 1 hour is associated with absorption events, and, at that, caused by high-energy precipitation, since the riometer is within the auroral oval and receives at 40MHz. Furthermore variation in cosmic noise itself over timescales of hours is slow, and particularly so for an instrument averaging signal of a large part of the sky at high latitude (a narrow beam riometer would respond to more discrete signals and detect shorter term variability). If the reader is unfamiliar with ionospheric physics, clarification can be obtained by reading appropriate chapters in (e.g.) Hargreaves (1979 and 1992) and the recent study by Kellerman et al. (2014) contains an exhaustive source of references. For periods > 1 day, variation of the signal is largely predicable from the geometry of the rotation of the observation point relative to the galaxy. Nevertheless, solar activity responsible for polar cap absorption events can persist for consecutive days and the associated absorption is modulated by the Earth's rotation and compounded by ion chemistry. For the shortest timescales before the onset of the approximately white instrumental noise described earlier, it is somewhat unclear as to which processes are responsible for the less steep (\sim unity) spectral exponent. It will be instructive to convert the spectral exponents (β) to generalized Hurst exponents (α) for comparison with similar analyses of potentially related solar and terrestrial metrics. A major assumption here, therefore, is that a single exponent is an appropriate descriptor of the data: no underlying theory exists suggests that a single spectral exponent is the correct functional form. The methodology simply follows that used by similar investigations of solar/ionospheric time series (references herein) and this caveat should be kept in mind when

considering the results that follow. For periods > 1 day, $\alpha = 0.94 \pm 0.04$; for periods > 1
 hour, $\alpha = 1.24 \pm 0.01$; for periods > 1 minute, $\alpha = 0.86 \pm 0.00$, uncertainties having been
 275 propagated from the fitting to the spectrum described earlier (Taylor 1982). These values
 indicate that the $>$ hour subrange is characterised by non-persistent fractional Brownian
 motion (fBm) whereas the other subranges either side are characterized by (marginally)
 fractional Gaussian noise (fGn) or approximately $1/f$ fluctuations. For longer period
 variability the hypothesis that the spectral exponent is relatively unrelated to high energy
 280 particle precipitation is supported by good agreement with the results of Canal et al. (2012)
 who report $1/f$ scaling for low energy secondary cosmic ray flux at low frequencies. On the
 other hand, Canal et al. (2012) find sunspot variation for periods less than 1 month to be
 characterized by $\beta \approx 1.4$, or $\alpha \approx 1.2$. This is the same as the $>$ hours value reported here (viz.
 1.24). Solar activity can be parameterized by a number of metrics including sunspot number
 285 and of course is the ultimate cause of ionospheric enhancements that give rise to riometer
 response at these timescales. It is interesting to note that a plethora of investigations of
 scaling in parameters related to auroral activity in the auroral oval (i.e. on average
 equatorward of 79°N) indicate, although not exclusively, generalized Hurst exponents
 somewhat larger than reported here and suggestive of persistent fBm. One example is an
 290 analysis of Disturbance storm time (*Dst*) index by Balasis et al. (2006), reporting scaling in
 the range (5 days -2 h) with α between ~ 1.4 and ~ 1.6 . For the geomagnetic field in the auroral
 oval, Hall (2014b) similarly reports α between ~ 1.39 and ~ 1.54 and Hamid et al. (2009)
 assert that for active days the geomagnetic activity scales with $\alpha > 1.5$.

In summary, three spectral subranges can be identified apart from the white noise deemed
 295 instrumental: a short timescale regime of the order of minutes to hours, exhibiting $1/f$ scaling,
 an intra-day timescale with a spectral slope of ~ 1.4 , and finally a longer timescale regime

also exhibiting $1/f$ scaling. For the first of these, it is difficult to identify a specific underlying physical process. For the second, similarity with intra day variability in the geomagnetic field (c.f. Hall, 2014b; Pulkkinen et al.2006; Wanliss and Reynolds, 2003; Takalo et al., 1994; hamid et al., 2009) and with solar disturbances (c.f. Balasis et al., 2006; Rypdal and Rypdal, 2010 and 2011) suggests solar origins and therefore cosmic noise absorption. The last spectral regime has similarities with slow fluctuations in independent determinations of cosmic ray intensity therefore suggesting origins in cosmic ray sources (c.f. Canal et al., 2012; Forbush, 1954 and 1958).

305 **Conclusions**

Cosmic noise signal at 40MHz has been recorded at 79°N, 12°E within the polar cap, providing, for this study, a time-series of approximately 18 months at 2 sec resolution. Examinations of probability density function and quantile-quantile plots reveal that the data can hardly be described by a Gaussian distribution, and that a Cauchy model fits better, thus suggesting an underlying Lévy process of some form. As explained earlier, the Cauchy distribution is only hypothesized here, based on the identification of Lévy processes in solar and ionospheric observables; multiple processes could be operating, which would be hard to identify unambiguously with the methods used here. However, the power spectral density indeed exhibits spectral subranges with differing scaling properties. The minute-to-hour fluctuations are characterized by $1/f$ scaling, the physical meaning of which is difficult to identify. The hour-to-day fluctuations are characterized by a spectral exponent of ~ 1.4 corresponding to a generalized Hurst exponent of 1.24 suggestive of anti-persistent fractional Brownian motion; these are associated with absorption - reduction of cosmic noise signal due to the intervening ionosphere in turn modulated by solar activity. Fluctuations longer than \sim day timescales are characterized by $1/f$ scaling and comparison with other studies supports a

hypothesis that cosmic noise intensity itself - i.e. independent of the intervening ionosphere, is responsible. Key products transpire from this study:

(a) Solar variability and its interaction with the terrestrial ionosphere is popularly known as “space weather”. The ionospheric response has typical timescales of hours, but may repeat
325 over consecutive days due to the Earth’s rotation, and over weeks due to the Sun’s rotation. Signal variation with scales of ~hours to days contains information on cosmic noise absorption and are therefore relevant for space weather considerations. Shorter timescales contain information relating to other physical processes including characteristics of the instrument itself and characterization can be a useful tool for exclusion of non-geophysical
330 data. Longer timescales contain information on the instrument’s view of the galactic sources, predominantly modulated by the Earth’s rotation and orbit, but also possible variation in the source itself.

(b) Underlying physical processes can be identified in riometer data by classification in terms of the generalized Hurst exponent. The study here therefore contributes to the growing
335 arsenal of links between similar classifications with links to physical processes originating outside the solar system, in solar-terrestrial relations, and even in the neutral atmosphere including possible anthropogenic forcing.

Subsequent investigation could include examination of cosmic noise signals at both 30 and 40 MHz, with their respective responses to precipitating particle energies, from receivers
340 within, under and outside the aurora oval, together with corresponding magnetometer analyses. Such results would be valuable to substantiate the aforementioned hypotheses but more importantly to establish dependence of the spectral characteristic on geomagnetic latitude and energies of precipitating particles.

345 **Acknowledgements.** Data from the Ny-Ålesund station can be obtained via Tromsø
Geophysical Observatory.

References

- Balasis, G., Daglis, I. A., Kapiris, P., Vassiliadis, D., and Eftaxias, K.: From pre-storm
 350 activity to magnetic storms: a transition described in terms of fractal dynamics, *Ann. Geophys.*, 24, 3557-3567 2006.
- Behera, J. K., Sinha, A. K., Singh A. K., Rawat, R., Vichare, G., Dhar, A., Pathan, B. M.,
 Nair, K. U., Selvaraj, C. and Elango, P.: First results from imaging riometer installed at
 Indian Antarctic station Maitri, *J. Earth Syst. Sci.*, 123(3) 593-602, 2014.
- 355 Chambers, J. M., Cleveland, W. S., Kleiner, B., and Tukey P. A.: *Graphical Methods for Data Analysis*. 395pp., Duxbury Press, Boston, Massachusetts, 1963.
- Canal, C. A. G., Hojvat, C., and Tarutina, T.: Scaler mode of the Auger Observatory and
 sunspots, *Astrophys. J. Suppl.*, 202, 16-22, doi: 10.1088/0067-0049/202/2/16, 2012.
- Delignieres, D., Ramdani, S., Lemoine, L., Torre, K., Fortes, M., and Ninot, G.: Fractal
 360 analyses for 'short' time series: A re-assessment of classical methods, *J. Mathematical Psychology*, 50, 525-544, 2006.
- Eichner, J. F., Koscielny-Bunde, E., Bunde, A., Havlin, S., and Schnellhuber, H.-J.: Power-
 law persistence and trends in the atmosphere: A detailed study of long temperature
 records, *Phys. Rev. E*, 68, 046133, doi:10.1103/PhysRevE.68.046133, 2003.
- 365 Eke, A. H., Hermán, P., Bassingthwaighte, J. B., Raymond, G. M., Percival, D. B., Cannon,
 M., Balla, I., and Ikrényi, C.: Physiological time series: Distinguishing fractal noises from
 motions, *Pfügers Archives*, 439, 403-415, 2000.
- Forbush, S. E.: World-wide cosmic-ray variations 1937-1952, *J. Geophys. Res.*, 59(4), 525-
 542), 1954.

- 370 Forbush, S. E.: Cosmic-ray intensity variations during two solar cycles, *J. Geophys. Res.*,
63(4), 651-669, 1958.
- Fougère, P. F.: On the accuracy of spectrum analysis of red noise processes using maximum
entropy and periodograms methods: Simulation studies and application to geographical
data, *J. Geophys. Res.*, 90, 4355-4366, doi:10.1029/JA090iA05po4355, 1985.
- 375 Grassberger, P., and Procaccia, I.: Measuring the strangeness of strange attractors, *Physica D*,
9(1-2), 189-208, 1983.
- Hall, C. M.: Complexity signatures for short time scales in the atmosphere above
Adventdalen, Svalbard, *J. Geophys. Res. Atmos.*, 119, doi:10.1002/2013JD020988, 2014a.
- Hall, C. M.: Complexity signatures in the geomagnetic H-component recorded by the Tromsø
380 magnetometer (70°N, 19°E) over the last quarter of a century, *Nonlin. Processes Geophys.*,
21, 1051-1058, doi:10.5194/npg-21-1051-2014, 2014b.
- Hamid, N. S. A., Gopir, G., Ismail, M., Misran, N., Hasbi, A. M., Usang, M. D., and Yumoto,
K.: The Hurst exponents of the geomagnetic horizontal component during quiet and active
periods, in: *Proc, 2009 Int. Conf. on Space Sci. and Comm.*, IEEE publishing, US and
385 Canada, 26-27 October 2009, Port Dickson, Malaysia, 186-189, 2009.
- Hargreaves, J. K.: *The Upper Atmosphere and Solar-Terrestrial Relations*, 298pp., Van
Nostrand Reinhold Co Ltd., Wokingham, England, 1979.
- Hargreaves, J. K., *The Solar-Terrestrial Environment*, 420pp., Cambridge University Press,
Cambridge, England, 1992.
- 390 Hartmann, A., Mukli, P., Nagy, Z., Kocsis, L., and Hermán, P.: Real-time fractal signal
processing in the time domain, *Physica A*, 392, 89-102, 2013.

- Heneghan, C., and McDarby, G.: Establishing the relation between detrended fluctuation analysis and power spectral density analysis for stochastic processes, *Phys. Rev. E*, 62(5), 6103-6110, 2000.
- 395 Hurst, H. E.: Long-term storage of reservoirs: an experimental study, *Trans. American Soc. of Civ. Eng.*, 116, 770-799, 1951.
- Kantelhardt, J. W., Koscielny-Bunde, E., Rybski, D., Braun, P., Bunde, A., and Havlin, S.: Long-term persistence and multifractality of precipitation and river runoff records, *J. Geophys. Res.*, 111, D01106, doi:10.1029/2005JD005881, 2006.
- 400 Kellerman, A. C., Shprits, Y. Y., Makarevitch, R. A., Spanswick, E., Donovan, E., and Reeves, G.: Characterization of the energy-dependent response of riometer absorption, *J. Geophys. Res. Space Physics*, 120, 615-631, doi:10.1002/2014JA020027, 2014.
- Koscielny-Bunde, E., Bunde, A., Havlin, S., Roman, H. E., Goldreich, Y., and Schnellhuber, H.-J.: Analysis of daily temperature fluctuations, *Phys. Rev. Lett.*, 81(3), 405 729-732, 1998.
- Lennartz, S., and Bunde, A.: Trend evaluation in records with long-term memory: application to global warming, *Geophys. Res. Lett.*, 36, L16706, doi:10.1029/2009GL039516, 2009.
- Little, C. G., and Leinbach, H.: The riometer - a device for the continuous measurement of ionospheric absorption, *Proc IRE*, 47, 315-320, doi: 10.1109/JRPROC.1959.287299, 1959.
- 410 Mandelbrot, B. B.: *The fractal geometry of nature*, W. H. Freeman & Co, New York, 495 pp., 1983.
- Mandelbrot, B. B., and van Ness, J. W.: Fractional Brownian motions, fractional noises and applications, *SIAM Review*, 10, 422-437, 1968.

- Peng, C. K., Mictus, J., Hausdorff, J., Havlin, S., Stanley, H.E., and Goldberger, A.L.: Long-
415 range anticorrelations and non-Gaussian behavior of the heartbeat, *Phys. Rev. Lett.*, 70,
1343-1346, 1993.
- Press, W. H., and Rybicki, G. B.: Fast algorithm for spectral analysis of unevenly sampled
data, *The Astronomical J.*, 338, 277-280, 1989.
- Pulkkinen, A., Klimas, A., Vassiliadis, D., Uritsky, V. and Tanskanen, E.: Spatiotemporal
420 scaling properties of the ground geomagnetic field variations, *J. Geophys. Res.*, 111,
A03305, doi:10.1029/2005JA011294, 2006.
- Rypdal, M., and Rypdal, K.: Stochastic modeling of the AE index and its relation to
fluctuations in B_z of the IMF on time scales shorter than substorm duration, *J. Geophys.*
Res., 115, A11216, doi:10.1029/2010JA015463, 2010.
- 425 Rypdal, M., and Rypdal, K.: Discerning a linkage between solar wind turbulence and
ionospheric dissipation by a method of confined multifractal motions, *J. Geophys. Res.*,
116, A02202, doi:10.1029/2010JA015907, 2011.
- Scafetta, N., and West, B. J.: Solar flare intermittency and the Earth's temperature anomalies,
Phys. Rev. Lett., 90, 248701-1-248701-4, 2003.
- 430 Sato, K.: Lévy processes and infinitely divisible distributions, *Cambridge Studies in*
Advanced Mathematics, 68, Cambridge University Press, Cambridge, 1999.
- Takalo, J., Timonen, J. and Koskinen, H.: Properties of AE data and bicolored noise, *J.*
Geophys. Res., 99, 13239-13249, 1994.
- Taylor, J. R.: *An Introduction to Error Analysis*, University Science Books, Sausalito,
435 California, ISBN 0-935702-75-X, 327 pp., 1982.

Wanliss, J. A. and Reynolds, M. A.: Measurement of the stochasticity of low-latitude geomagnetic temporal variations, *Ann. Geophys.*, 21, 2015-2030, 2003.

Watkins, N. W., Credgington, D., Hnat, B., Chapman, S. C., Freeman, M. P., and Greenhough, J.: Towards synthesis of solar wind and geomagnetic scaling exponents: a
440 fractional Lévy motion model, *Space Sci. Rev.*, 121, 271-284, 2005.

Wilk, M. B., Gnanadesikan, R.: Probability plotting methods for the analysis of data, *Biometrika* (Biometrika Trust) 55 (1): 1–17, 1968.

445

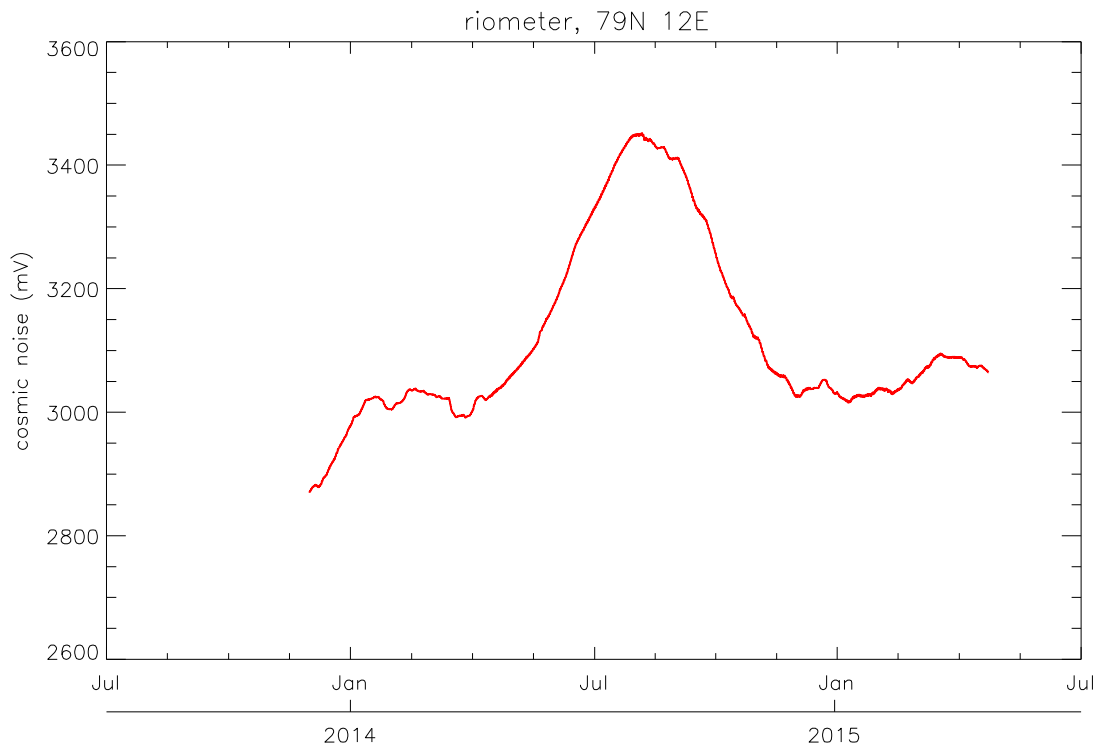


Fig. 1. Cosmic noise at 40MHz measured by riometer at Ny-Ålesund, 79°N, 12°E. Original data at 2 sec time resolution have been smoothed by a 1-month boxcar to show both the overall data coverage and seasonal variation.

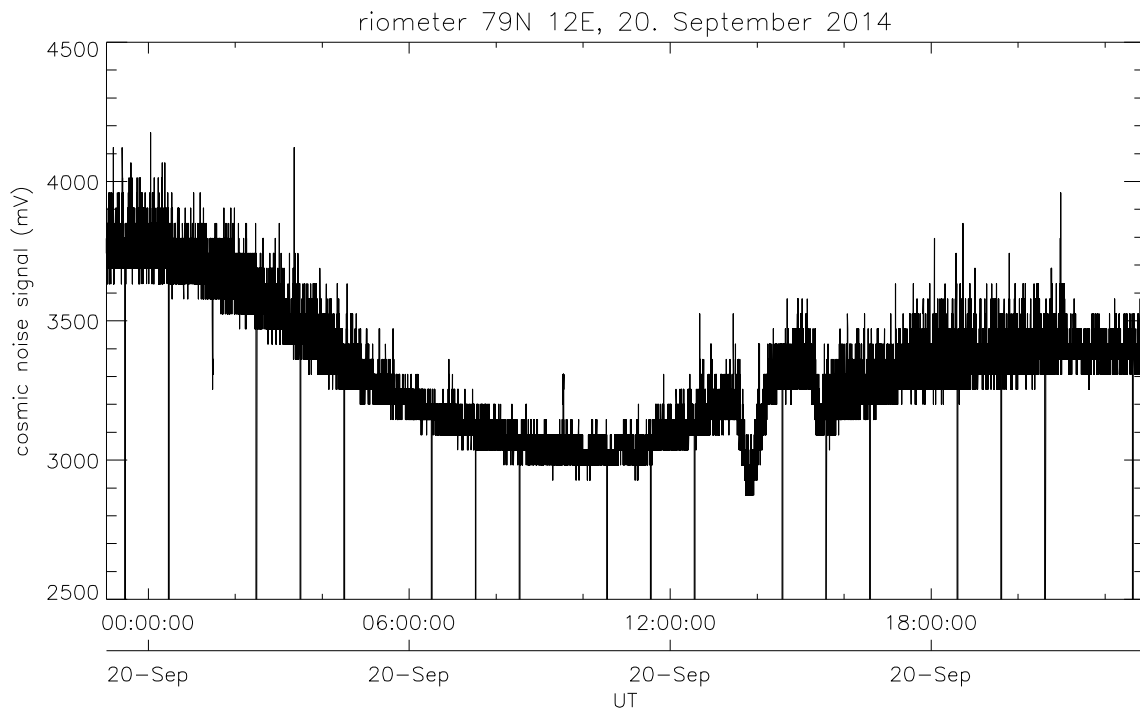
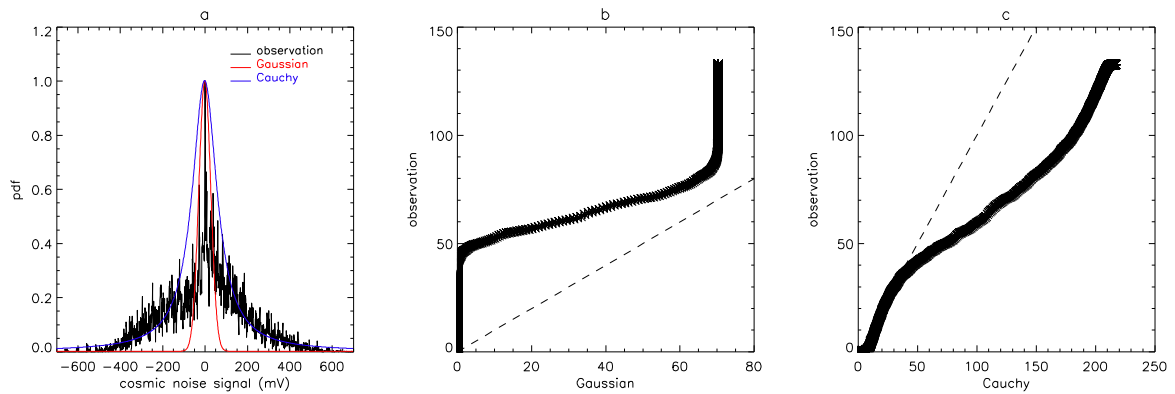


Fig. 2. Detail plot of cosmic noise at 40MHz measured by riometer at Ny-Ålesund, 79°N, 12°E for 20 September 2014. Original samples are shown, including the hourly calibration points.



460 Fig. 3. Portrayals of the distribution of the stochastic component (described in the text) of the
 cosmic noise signal. Left: probability density function with fitted Gaussian (red) and
 Cauchy (blue) distributions superimposed (explained and discussed in the text). Centre:
 Q-Q plot of the observed data versus Gaussian; right: Q-Q plot of the observed data
 versus Cauchy.

465

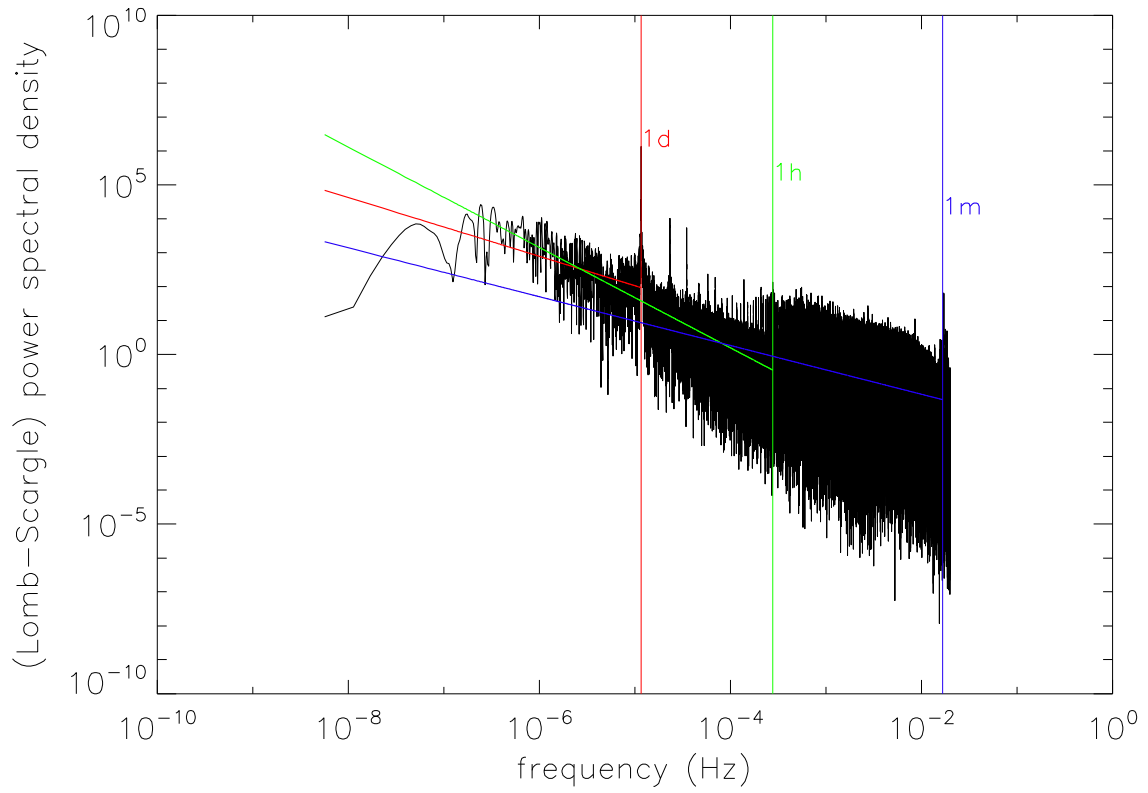


Fig. 4. Spectral analysis for data shown in previous figures. Familiar timescales are indicated

470

by vertical dotted/dashed lines. Fitted scaling exponents are shown by coloured lines.